Cerebral Cortex November 2011;21:2482–2497
doi:10.1093/cercor/bhr020
Advance Access publication March 31, 2011

Saccade-Related Modulations of Neuronal Excitability Support Synchrony of Visually Elicited Spikes

Junji Ito[1], Pedro Maldonado[2], Wolf Singer[3] and Sonja Grün[1,4]

[1]Laboratory for Statistical Neuroscience, RIKEN Brain Science Institute, Wako, 351-0198 Saitama, Japan, [2]CENI and Programa de Fisiología y Biofísica, ICBM, Facultad de Medicina, Universidad de Chile, Santiago 8380453, Chile, [3]Department of Neurophysiology, Max-Planck Institute for Brain Research, D-60528 Frankfurt/M, Germany

[4]Current address: Institute of Neuroscience and Medicine (INM-6), Computational and Systems Neuroscience, Research Center Jülich, 52425 Jülich, Germany

Address correspondence to Dr Junji Ito, Laboratory for Statistical Neuroscience, RIKEN Brain Science Institute, 2-1 Hirosawa, Wako, 351-0198 Saitama, Japan. Email: j-ito@brain.riken.jp.

During natural vision, primates perform frequent saccadic eye movements, allowing only a narrow time window for processing the visual information at each location. Individual neurons may contribute only with a few spikes to the visual processing during each fixation, suggesting precise spike timing as a relevant mechanism for information processing. We recently found in V1 of monkeys freely viewing natural images, that fixation-related spike synchronization occurs at the early phase of the rate response after fixation-onset, suggesting a specific role of the first response spikes in V1. Here, we show that there are strong local field potential (LFP) modulations locked to the onset of saccades, which continue into the successive fixation periods. Visually induced spikes, in particular the first spikes after the onset of a fixation, are locked to a specific epoch of the LFP modulation. We suggest that the modulation of neural excitability, which is reflected by the saccade-related LFP changes, serves as a corollary signal enabling precise timing of spikes in V1 and thereby providing a mechanism for spike synchronization.

Keywords: free viewing, local field potential, phase locking, primary visual cortex, spike synchrony

Introduction

When primates visually explore their surroundings or examine an image, they make rapid eye movements (saccades) 3–4 times a second. During each visual fixation, complex visual computations and the preparation for the next eye movement are accomplished in as little as 120 ms (Kirchner and Thorpe 2006). V1 neurons exhibit transient changes in firing rates during exposure to complex scenes and these rates are characteristically low compared with the response to parameterized and spatially confined stimuli such as bars, gratings, or Gabor patches (Gallant et al. 1998; Vinje and Gallant 2000; Olshausen and Field 2005; MacEvoy et al. 2008; Maldonado et al. 2008).

Based on the evidence that processing of visual information is surprisingly fast, theoretical work had proposed that information may not be encoded solely in variations of firing rates but also in the precise and coordinated timing of action potentials. In particular, it was proposed that the timing of the very first spikes arriving at early stages of the visual system after stimulus presentation plays a special role (VanRullen and Thorpe 2002; Kupper et al. 2005). In a recent study, we investigated this proposal and found that the spike responses of V1 neurons during free viewing are synchronized just around the onset of the postsaccadic rate increase (Maldonado et al. 2008).

It has been suggested that a corollary signal arriving in V1 simultaneously with saccade initiation could serve as a temporal reference for the spikes induced by the visual input (Singer 1977; Jeannerod et al. 1979). A possible candidate for such a signal could be the saccade-related changes in neuronal excitability that manifest themselves as modulations of the local field potential (LFP) or current source density (CSD) profiles (Bartlett et al. 1976; Rajkai et al. 2008; Bosman et al. 2009; for a review, see Melloni et al. 2009). Rajkai et al. (2008) reported that the oscillations of neuronal excitability in monkey V1 were phase locked to the onset of fixations during voluntary eye movements performed in the dark, so that the excitability becomes maximal around the time when visual signals should have arrived if the animals were in a lighted environment. Bosman et al. (2009) reported that microsaccades during prolonged fixations evoke (or phase reset) LFP oscillations, which acts as a mechanism to enhance the neuronal response to the changes in the retinal image due to the fixational eye movements. Both of these studies clearly show that the brain uses a nonvisual, eye movement–related signal to "predictively" prepare the visual system for processing of the visual inputs that occur at each fixation.

On the other hand, it has recently been shown that spike timing can be adjusted by oscillatory modulations of neuronal excitability and locked to a specific phase of the oscillation (O'Keefe and Recce 1993; Volgushev et al. 1998; Csicsvari et al. 2003; Jacobs et al. 2007). Other studies have reported functional relevance of such phase locking of spikes in the visual cortex (Lee et al. 2005; Montemurro et al. 2008) as well as in other brain areas (Huxter et al. 2008; Kayser et al. 2009).

Taken together, these previous studies point toward a proposition that eye movement–related changes in neuronal excitability may work as a mechanism for the precise coordination of the timing of early visually evoked spikes during free viewing, as observed in Maldonado et al. (2008). Therefore, in this study, we examine the spiking activity and the simultaneously recorded LFP in V1 while monkeys freely view natural images and perform self-initiated eye movements. We extend the finding in Rajkai et al. (2008) and Bosman et al. (2009) to the condition of free viewing of natural images and relate the timing of visually evoked single spikes to the LFP modulations related to the initiation of voluntary eye movements on a trial-by-trial basis.

Materials and Methods

Data Collection

All experiments followed institutional and NIH guidelines for the care and use of laboratory animals. Two adult, male capuchin monkeys

(*Cebus apella*) weighing 3–4 kg served as subjects for this study. Henceforth, these animals are referred to as monkey D and S. Under sterile conditions, each animal was implanted with a scleral search coil for monitoring eye position (Judge et al. 1980) and a cranial post for head fixation. After a period of visual fixation training, we performed a second surgical procedure, in which a plastic recording chamber was mounted over the visual cortex. Area 17 was accessed by stereotaxic coordinates (Gattass et al. 1987). A micromanipulator with up to 8 independently movable tetrodes could be attached to the chamber. After a small craniotomy was performed, an incision was made in the dura mater and the guide tube array was positioned over the cortical surface. After the animals participated in the recordings, their head post, eye coils, and manipulator were removed, and they were donated to a local zoo. During the recording, the animals were seated in a chamber dimly lit at a low scotopic level (1–2 lx, LX-110 Lux Meter). They were presented with a collection of 13 pictures of different natural scenes (consisting of pictures of animals, faces and landscapes, 800 × 600 pixel resolution; taken from Corel photo library), which were displayed on a computer monitor (frame rate: 60 Hz) located 57 cm in front of the animals subtending 40 × 30° of visual angle. As a control, for every third stimulus presentation, a blank frame with black background was presented instead of a natural image. We refer to the trials with natural image stimuli as image condition trials and those with the blank frame as blank condition trials. In order to maintain the alertness of the animals, before every trial, we forced them to perform a fixation task, where a black frame with a single central fixation spot was presented and they had to fixate to it (1° window) for 1 s in order to be rewarded (referred to as fixation part). Then, the natural images or the blank frame were presented for 3 or 5 s for monkey D or S, respectively (free-viewing part). In the free-viewing part, the animals were allowed to freely explore the monitor screen with self-initiated eye movements (Fig. 1*A*), while the experimental protocol required the animals to maintain their gaze within the limits of the monitor for the 3- or 5-s presentation period, to be rewarded with a drop of juice. After a free-viewing part, another fixation part began, followed by the next free-viewing part, and so forth. This process was repeated as long as the animals were motivated to continue the task. Only the data from the free-viewing part with successful gazes served for the following analyses.

Recording of Eye Position and Extraction of Eye Movement Events

Vertical and horizontal eye positions were monitored (Fig. 1*B* top) with a search coil driver (DNI Instruments, Resolution: 1.2 minutes of arc) and then digitized at 2 kHz. To extract the different types of eye movements from the eye traces, we developed an automatic algorithm (coded in *C*) based on the following definitions of eye movement events. Saccades were defined as eye movements with an angular velocity higher than 100°/s lasting for at least 5 ms. In addition, saccades were required to exhibit a minimum acceleration of 170°/s^2. Fixation periods were classified as such when they lasted at least 100 ms with the eye position maintained within 1° of the gaze location reached at the end of a saccade. Sustained movements with angular velocities ranging from 70 to 150°/s, and durations of at least 100 ms were classified as drifts, during which we did not analyze the data in the present study. Only the unambiguous fixation periods that were initiated and terminated by unambiguous saccades were considered for further analysis. We call each combination of a saccade and the immediately following fixation period as a "saccade–fixation (S–F) trial." By this definition, an S–F trial begins with a saccade-onset (corresponding to the end of the preceding fixation), followed by a saccade-offset, which is equivalent to fixation-onset and ends with a fixation-offset. The total number of S–F trials was 2452 for monkey D and 2686 for monkey S.

Electrophysiological Recordings

Neuronal activity in the primary visual cortex during the free-viewing task was recorded with an array of 8 individually adjustable custom fabricated nichrome tetrodes (1–2 MΩ impedance). The electrodes were positioned in a circular array, with a center-to-center distance of ~400 μm. The signals were amplified (10 K), separated into multiunit activity (MUA; 0.5–5 kHz) and LFPs (1–200 Hz) by band-pass filtering and then stored in an electronic device at 25 kHz and 3 kHz sampling rates, respectively. Only one LFP signal was selected from 1 of the 4

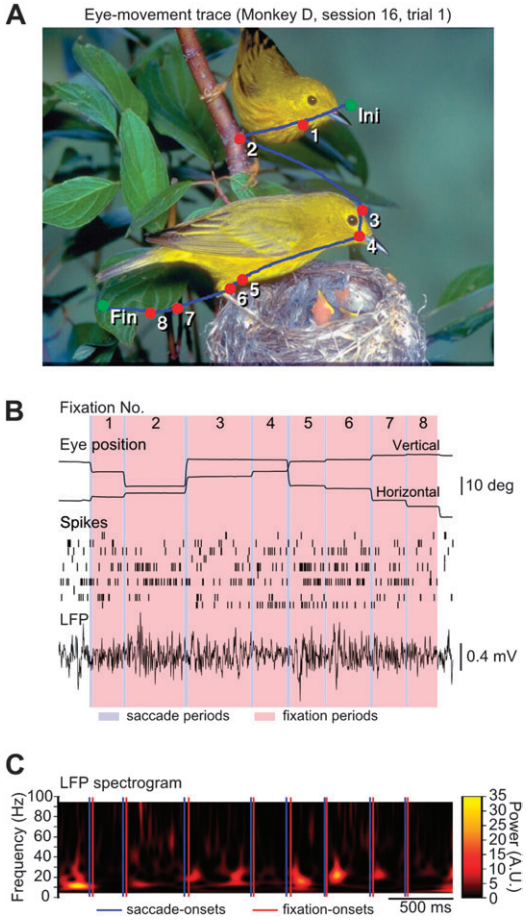

Figure 1. Eye movements and V1 activity during free viewing of a natural image. (*A*) Trace of eye movements of monkey D on 1 of 13 presented images. Red dots indicate fixation positions and blue curves represent the traces of saccadic eye movements. Green dots indicate the initial (Ini) and final (Fin) eye positions in this trial. (*B*) Traces of the horizontal and vertical eye positions (top) are shown together with the simultaneously recorded single unit spike trains of 10 neurons (middle) and an LFP trace (3–100 Hz; bottom) from one of the tetrodes. Periods of fixations and saccades are indicated by red and blue shaded areas, respectively. Fixation periods are numbered according to the order of their occurrence so that they correspond to the numbers in (*A*). (*C*) Spectrogram (in a frequency range from 5 to 95 Hz) of the LFP trace shown in (*B*) calculated using the wavelet transform. The onsets of fixations and saccades are indicated by red and blue vertical lines, respectively. The power is given in arbitrary units.

channels of each tetrode. A notch filter was applied to the LFP signals in order to remove hum noise (at 50 Hz from the power line and at 60 Hz from the monitor refreshing rate). To observe a single trial LFP activity in a frequency-resolved manner, we applied wavelet transform to a LFP trace recorded during a presentation of one of the natural image stimuli (Fig. 1*C*). We used a Morlet wavelet defined at frequency f and time τ by $\sqrt{f} \cdot \exp[i2\pi f(u-\tau)] \exp[-(u-\tau)^2/(2\sigma^2)]$, according to Le Van Quyen et al. (2001). The parameter σ was set to $5/(6f)$, so that the wavelet contains about 5 wave cycles. The MUA signals were fed through an off-line sorting program (Gray et al. 1995) to reconstruct the spike trains of single units recorded simultaneously by a single tetrode. On successive penetrations (i.e., recording sessions) through the same guide tube, recordings were resumed always at least 200 μm deeper than during the previous recording session. This sampling procedure was continued until activity could no longer be measured, and then the guide tubes were repositioned. We identified 153 single units from 26 recording sessions for monkey D and 251 units from 51 sessions for monkey S. Some penetrations crossed V1 twice in the anterior part of the calcarine sulcus, which led to systematic changes in receptive field (RF) position. The location of the RF of a multiunit response at one

individual tetrode was assessed by hand mapping using a mouse-driven white bar, while the animals fixated on a small fixation point in the middle of the screen. Because all tetrodes were close to each other, multiunit RFs largely overlapped.

Event-Triggered LFP Averages

To study LFP activities in response to eye movements, we calculated LFP averages either triggered on the onset of fixations or on the onset of saccades (Fig. 2*C,D*). For this calculation, we first band-pass filtered the recorded LFP signals between 1 and 100 Hz, by eliminating the frequency components outside this range in the Fourier space before inversely transforming the residual components back to the time domain. For calculating the fixation-onset–triggered LFP average, we extracted from each S–F trial (12408 for Monkey D and 8585 for Monkey S) a 300-ms segment of the filtered LFP signal (–100 to 200 ms relative to fixation-onset) and averaged them. To access the variance of the LFPs across trials, we calculated the standard error at each time bin. These calculations were performed at the time resolution of the sampling frequency of 3 kHz. The saccade-onset–triggered average was calculated in the same manner except that saccade-onsets were used as the reference time point for extracting the LFP segments.

Event-Triggered Mean Firing Rate

To derive the firing rate responses in relation to the eye events, we computed the mean firing rates of all neurons across all S–F trials aligned either to saccade- or to fixation-onset (Fig. 2*A,B*). Before averaging, the spike trains were smoothed by convolution with a Gaussian kernel of 4 ms standard deviation. Then segments of 300-ms duration (between –100 and 200 ms relative to the respective trigger event) were extracted and averaged to retrieve the smoothed population peri-stimulus time histogram (PSTH). As for the LFP average, the variability of the firing rate response is captured by the standard error calculated at each time bin on the same time resolution.

Phase Consistency of LFP Activity Across Fixations

The average LFP shows a clear sinusoidal waveform, indicating that the LFP modulation in response to the eye events is on a specific time scale. Deriving this time scale by direct application of a spectral analysis to the average LFP time series would lead to a very poor frequency resolution due to the limited duration (300 ms) of the time series. Therefore, we determined the time scale by employing a phase consistency analysis of the LFP responses across fixations in a frequency-resolved manner in the range between 1 and 100 Hz (Fig. 2*E,F*). To estimate the phase of the LFP activity for each frequency, we first applied a band-pass filter of a bandwidth defined by $\pm 0.2 \cdot f_c$ (Hz), with f_c, the center frequency of the filter, which is varied from 1 to 100 Hz in steps of 1 Hz. This definition of the bandwidth renders different frequency resolutions for different center frequencies, so that it allows a fine temporal resolution for a high center frequency and vice versa. (For example, the bandwidth for the center frequency of 10 Hz becomes 4 Hz [i.e., from 8 to 12 Hz], which is identical to the typical definition of the alpha frequency band.) We obtain the instantaneous phase of the filtered signal as the arc tangent of the ratio between the filtered signal and its Hilbert transform. The phase consistency of the

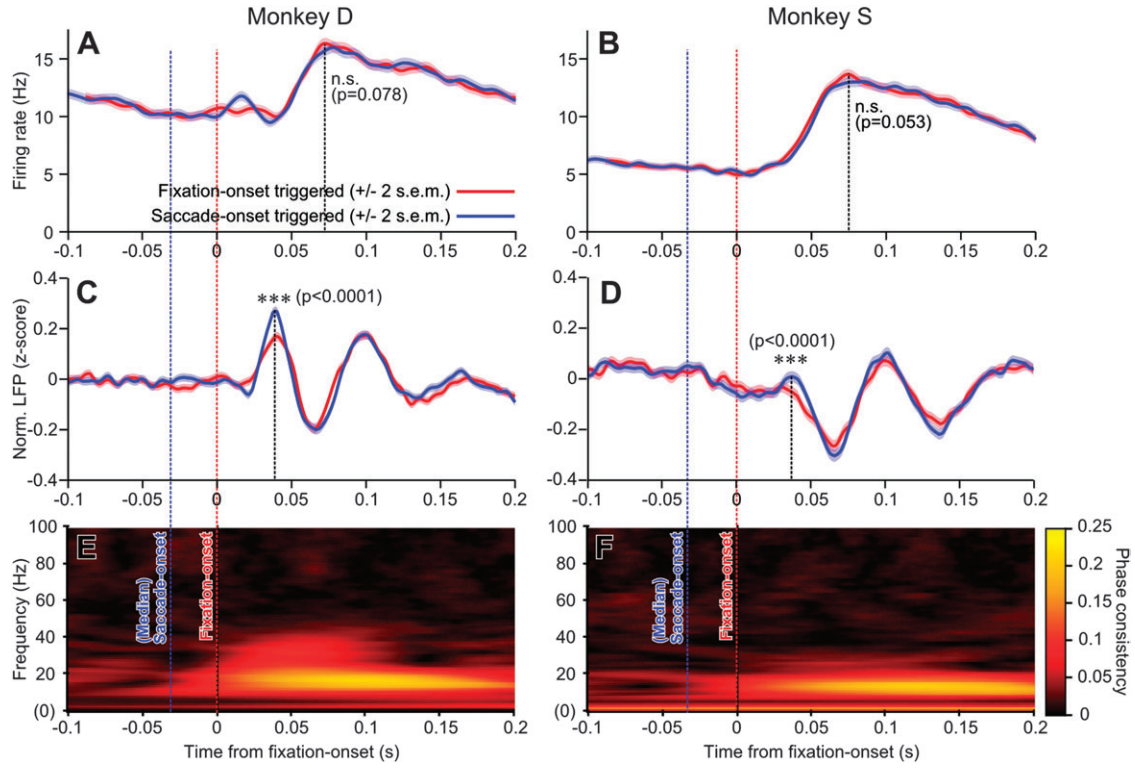

Figure 2. Spiking and LFP activities related to eye-event onsets during free viewing of natural images. Panels (*A,C,E*) and (*B,D,F*) show data of monkey D and S, respectively. (*A,B*) Mean firing rates triggered on fixation-onset (red) and saccade-onset (blue), estimated using a Gaussian kernel (standard of 4 ms). The color-shaded areas represent ±2 standard error of the mean (s.e.m.) of the respective signals. Spike data from all S–F trials and all recording sessions are combined. For better comparison, we plot saccade-onset–triggered and fixation-onset–triggered averages on a common time axis (here in relation to fixation-onset). Therefore, saccade-onset–triggered averages are shifted backwards in time by the median saccade duration (31 ms for monkey D and 33 ms for monkey S). Red and blue vertical lines indicate fixation-onset and typical saccade-onset timing, respectively. The significance of the difference between the peak responses of the 2 average rate profiles was assessed by testing if the mean of the trial-wise difference is significantly larger than zero (paired 2-tailed *t*-test). The 2 peak amplitudes were taken at time points 72 ms (*A*) and 74 ms (*B*) (black dashed lines) derived as the peak of the fixation-onset–triggered mean of the firing rate profiles. "n.s." indicates a nonsignificant difference. (*C,D*) LFP averages triggered on fixation-onset (red) and saccade-onset (blue). The color-shaded areas represent ±2 s.e.m. of the respective signals. The temporal alignment is the same as in (*A,B*). The significance of the trial-wise differences between the amplitudes of the first peaks of the 2 signals is derived by a 2-tailed *t*-test (as in *A,B*). The amplitude is taken at 40 ms (*C*) and 37 ms (*D*) (black dashed lines), which correspond to the peak position of the average LFP signals. "***" indicates that the 2 signals were significantly different with a *P* value smaller than 0.0001. (*E,F*) Phase consistency values of LFPs across S–F trials in the frequency range of 3–100 Hz (*y*-axis) as a function of time relative to fixation-onset (*x*-axis).

LFP signals across trials was obtained by calculating the vector average of the phases at any instant in time relative to the trigger event (i.e., fixation-onset or saccade-onset). The lengths of the resulting average vectors represent the phase consistency values. This procedure provides us with a measure of the reoccurrence of a specific phase of the signal at the same time relative to trigger onset across trials. Irrespective of the specific trigger event, the maximum phase consistency value was found during the LFP response at frequencies of f_c = 16 (image) and 7.5 (blank) (Hz) for monkey D and f_c = 13 (image) and 5.5 (blank) (Hz) for monkey S (Figs. 2*E,F* and 4*E,F*). The frequency extracted for each of the monkeys was considered in further analyses as their dominant LFP response frequency.

Saccade Duration–Resolved Averages of LFP and Firing Rates

To elucidate the temporal relationship between the eye movement events and the neuronal activities, we studied how the response latency of LFP and the firing rate depend on the duration of saccades. Therefore, we sorted S–F trials by saccade duration and calculated the respective fixation-onset–triggered averages of the LFPs for saccades of similar durations. Before averaging, the LFPs were band-pass filtered with a center frequency set to the respective dominant frequency. The result was smoothed across saccade durations with a sliding window (10-ms width) starting at saccade duration of 5 ms with 2 ms increments until 95% of the data were covered. We also computed the saccade duration-resolved firing rates accordingly. The obtained LFP and firing rate matrices are displayed in pseudocolor plots (Fig. 3) as a function of time (*x*-axis, representing the time relative to fixation-onset) and saccade duration (*y*-axis, representing saccade duration).

Phase-Locking Analysis

To examine whether or not the timing of the spikes is related to the LFP activity, we assessed the degree of temporal locking of the spikes to the phase of the LFP modulations. For this purpose, we measured the phase-locking value (PLV, Fig 4*A*). Thus, first we estimated the instantaneous phase of the LFP signals by applying the Hilbert transform (as done in the phase consistency analysis described above). Before the application of the Hilbert transform, the LFP signals were filtered with the bandwidth introduced above and around the center frequency f_c set to the monkey's dominant frequency, which differed in the different behavioral conditions (image and blank). For calculating the PLV, we extracted the phase values at the times of the simultaneously recorded spikes τ^i_{jk} that is, the timing of the *k*-th spike of cell *i* within the fixation period of the *j*-th S–F trial. The resulting phase values were denoted as $\Phi^i_{jk}=\Phi(\tau^i_{jk})$. Based on these, we calculated the PLV defined as $\left[\left(\sum_{i,j,k}\cos\Phi^i_{jk}\right)^2+\left(\sum_{i,j,k}\sin\Phi^i_{jk}\right)^2\right]^{1/2}/N$, where N is the total number of spikes taken into account. For the results presented in this study, we related spikes and LFPs recorded from the same electrode, however, comparable results were obtained when only signals from different electrodes were related.

We applied the phase-locking analysis either within a time window at a fixed position or in a sliding window fashion (Fig. 8) to yield the time

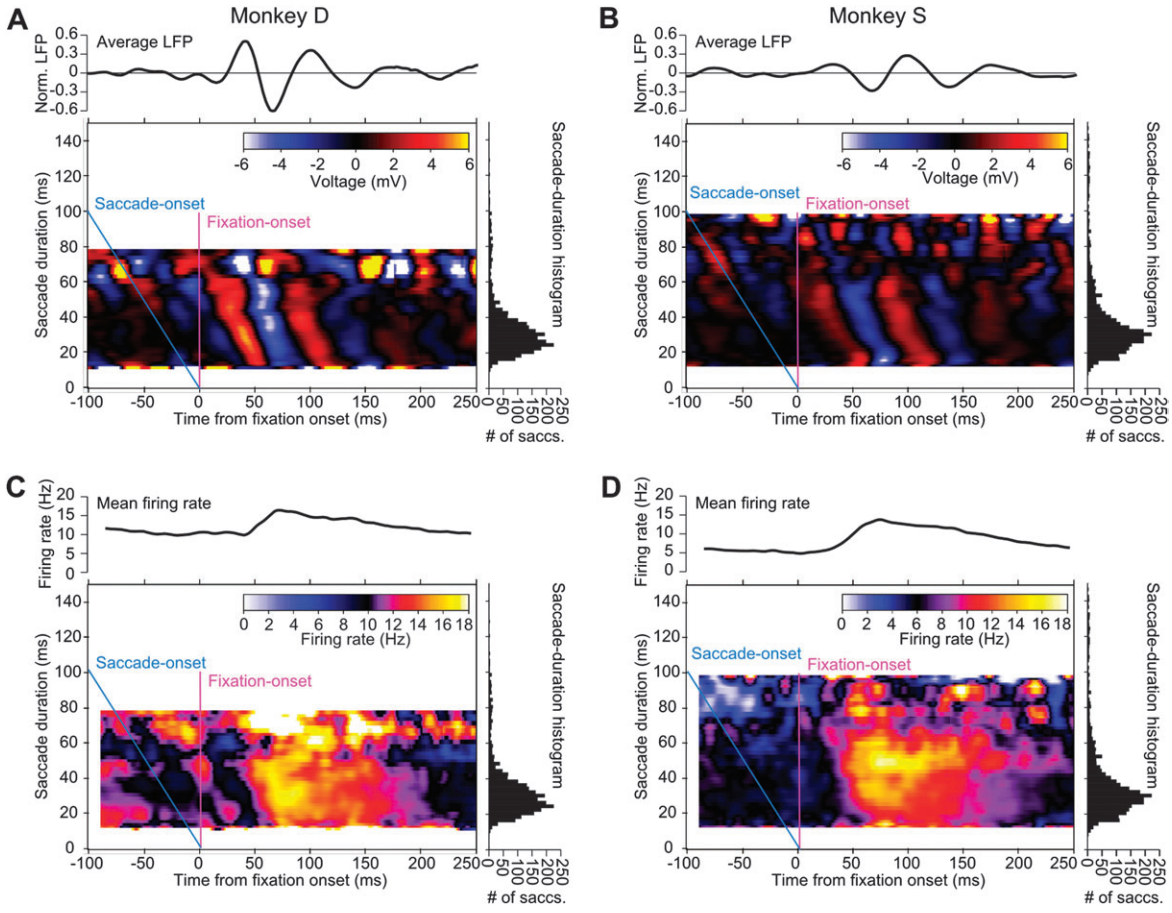

Figure 3. Saccade duration–resolved averages of LFP and firing rate during free viewing of natural images. Panels (*A,C*) and (*B,D*) show data of monkey D and monkey S, respectively. (*A,B*) Top: grand average LFP calculated from all S–F trials irrespective of the duration of saccades. Bottom: saccade duration–resolved average LFP (color coded). The LFP averages triggered on fixation-onset are calculated separately for subsets of S–F trials that fall within a 10-ms window of saccade duration. The *x*-axis represents time relative to fixation-onset, the *y*-axis represents the mean saccade duration of the S–F trials that contributed to the average at the corresponding vertical position. A histogram of the saccade durations (bin width: 2 ms) is shown to the right in each panel. Fixation-onset and saccade-onset times are marked by magenta and cyan lines, respectively. For better visibility, LFP signals were preprocessed with a band-pass filter ($\pm 0.2 \cdot f_c$ [Hz]) centered at the main frequency component f_c of the response activity (16 Hz for monkey D and 13 Hz for monkey S) before averaging. (*C,D*) Saccade duration–resolved mean firing rate displayed in the same manner as for (*A,B*).

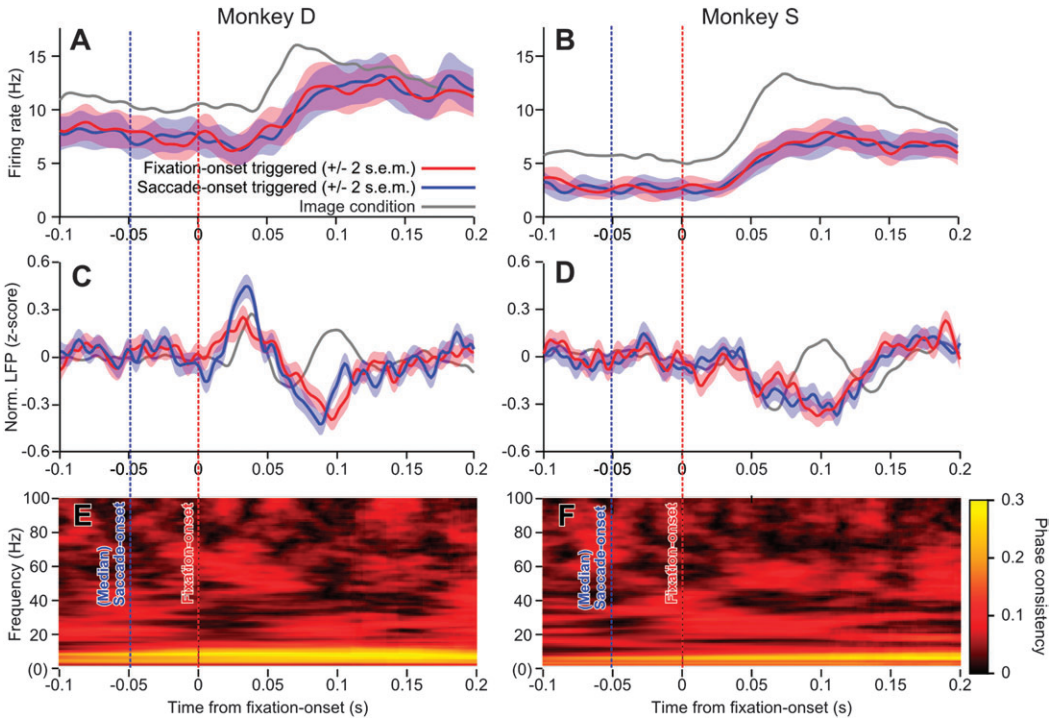

Figure 4. Firing rates and LFP activities related to eye-event onsets in the blank condition. The figure is organized in the same way as Figure 2, except for the gray curves in (*A–D*) that show the results for the image condition (fixation-onset–triggered average for firing rates and saccade-onset–triggered average for LFPs) for a better comparison.

dependence of the phase locking. In the former, the width of the window was set to one cycle of the dominant frequency to avoid a bias in the sampling of phase values and was centered at the peak of the fixation-onset–triggered average firing rate (Fig. 7*A,B*, yellow colored area). In the sliding window analysis, the window width was set to 20 ms and slid from 0 to 200 ms starting at fixation-onset. To explore a possible dependence of the PLV on the order of spikes during the fixation, we calculated the PLVs separately for the set of the first (1ST) and the second (2ND) spikes occurring after each fixation-onset and also for the set of all (ALL) spikes occurring during fixation periods (Fig. 7*C,E*). For cross-checking, we also repeated all the analyses based on an alternative phase estimation method (wavelet phase estimation, same method as described in Electrophysiological Recordings), which confirmed our results (not shown here).

Significance Test for Phase-Locking Value

We assessed the significance of PLV with 2 different surrogate methods: one is based on random shuffling of data and the other on random resampling of data.

Random Shuffling Surrogate

This surrogate method was employed both in the fixed time window and in the moving time window analyses of PLV. An inhomogeneous distribution of spikes (i.e., nonstationary firing rates) within the PLV analysis window may cause spuriously large PLVs due to a bias in the considered phase values. Similarly, if the width of the analysis window is shorter than one cycle of the dominant LFP frequency, only a restricted set of phase values is contained and thus may bias the resulting PLV. In order to avoid wrongly assigned significance to PLV estimates, we quantified the significance of the empirical PLV by comparison to a distribution of PLVs derived from surrogate data sets, which were generated by shuffling the spike trains of the individual neurons across different S–F trials (Fig. 6*B*). Thereby the spikes were related to LFPs of nonsimultaneous, randomly selected S–F trials. Each randomization generated one surrogate data set, which resulted in one surrogate PLV. The PLVs estimated from 10000 such surrogate data sets were used to construct a distribution of the surrogate PLVs to derive the *P* value Ψ of the PLV obtained from the original data. We quantified the significance by the surprise measure (SM) $S = \log[(1-\Psi)/\Psi]$ defined as (Palm et al. 1988; Fig. 7*D,F*). The trial shuffling procedure destroyed any possible correlation between the spike trains and the LFPs but preserved the potential sampling biases of spikes and phases within the analysis window. Thus, the obtained surrogate PLVs reflect the degree of phase locking resulting only from these biases. This approach yields a more conservative estimate of the PLV of the original data as compared with surrogates that do not preserve the biases inherent in the data, e.g., by spike time randomization.

Random Resampling Surrogate

This surrogate method was employed only in the PLV analysis with the fixed time window. In order to directly assess whether 1ST and 2ND spikes are significantly more strongly locked to the background LFP than arbitrarily selected spikes, we compared the SMs for 1ST and 2ND spikes with the SMs for arbitrarily chosen subsets of ALL spikes. For this purpose, we randomly picked from ALL spikes within the analysis time window the same number of spikes as 1ST or 2ND spikes and computed the SM of PLV for this subset of ALL spikes. We repeated this 1000 times and estimated the median and the 95 percentile of the SMs for the randomly resampled surrogate data sets. The SM for 1ST or 2ND spikes was considered to be significantly higher if it exceeded the 95 percentile of the corresponding surrogate.

Effect of LFP Amplitude on Phase Locking

To study the relationship between the amplitude of the LFP responses and the phase locking of spikes, S–F trials were separated into 2 groups (hi-peak and lo-peak group) according to the height of the first positive peak of the filtered LFP signal (filter details, see above) after fixation-onset. For deriving potential differences in the locking degree of the respective groups, we calculated separately for the 2 groups the time-dependent PLV (Fig. 9*B,C*) and the LFP averages (Fig. 9*D,E*).

Unitary Events Analysis

To examine the relation of the phase relation of spikes to the LFP and the occurrence of excess spike synchrony between neurons, we used the unitary events (UEs) analysis method for the detection of significant spike synchrony (Grün et al. 2002a, 2002b; Grün 2009). The method

enables to retrieve the time-resolved occurrence of excess spike synchrony and to relate its time course to the LFP modulations in response to eye events (Fig. 10). To evaluate UEs, we used the same approach as applied in our previous study (Maldonado et al. 2008), where it is outlined in detail. In brief: For each pair of simultaneously recorded neurons, we extracted the empirical number of coincidences (tolerated temporal jitter: 5 ms) from all trials within a given time window. To evaluate the significance of the detected number of coincidences, its count was compared with the number of coincidences expected on the basis of the firing rates of the neurons within the same time window. This expected number was derived as the sum of the trial-by-trial products of the firing probabilities of the 2 neurons, multiplied by the number of time steps within the window derived counts. The firing probabilities were estimated from the corresponding trial-by-trial spike counts within the window, normalized to the number of bins. The significance of the empirical count is derived as the *P* value estimated from a Poisson distribution with the mean set to the derived expected number. For a *P* value smaller or equal to a predefined significance level (here set to 0.05), the window is considered to contain UEs, that is, significant excess spike synchrony. The application of that procedure in a sliding window fashion (window size: 50 ms, increment: 1 ms) permits to extract the time-dependent UE rate for each neuron pair. The UE-PSTH in Figure 10, bottom, represents the UE rate averaged over all neuron pairs.

Results

Experiments

Using an array of 8 individually adjustable tetrodes, we recorded simultaneously the spiking activity, that is, discharges of multiple single neurons, and LFP signals from the primary visual cortex of 2 adult, male capuchin monkeys (*C. apella*). The animals (referred henceforth as D and S) were presented with a collection of 13 pictures of different natural scenes (an example image can be seen in Fig. 1*A*), as well as black, blank frames as a control. The animals were allowed to visually explore the images (or blank frames) by self-initiated eye movements, which were registered with the search coil technique (Judge et al. 1980). The experimental protocol only required that the animals maintain their gaze within the borders of the visual display.

A typical trace of eye movements during one presentation of an image is displayed in Figure 1*A* (blue curve). The time series of the horizontal and vertical eye positions during these eye movements (Fig. 1*B*, top) exhibited distinctive saccade and fixation periods. The onsets of the saccades and fixations were derived on the basis of the angular velocity and the acceleration of the eye movements (for details, see Materials and Methods). The median durations of saccades and fixations were 31 and 263 ms for monkey D and 33 and 371 ms for monkey S, respectively. The eye positions at the onsets of fixation periods are marked with red dots in Figure 1*A*. In the following, we refer to each successive pair of saccade and fixation periods as a saccade–fixation (S–F) trial.

Spiking and LFP Activities in Response to Eye Movements

We recorded up to 5 cells per tetrode from 68 recording sessions, yielding 418 single units individually identified by a manual clustering method (Gray et al. 1995). The RFs of most units were located within 5–10° from the center of gaze and were smaller than 2°. About 15% of the recordings were made below the opercular layer. No further RF properties were determined in order to save time for data acquisition during free viewing. As mentioned above, we also recorded LFP signals (1–200 Hz) from the same tetrodes. In Figure 1*B*, we show 10 spike trains and one LFP trace recorded concurrently with the eye movements shown in Figure 1*A*. The spectrogram of the LFP trace (Fig. 1*C*) indicates short-lasting power increases in the beta band (10–25 Hz) shortly after onsets of fixations.

To examine the changes of the spiking and LFP activities in relation to the eye movements, we computed separately for each of the animals the averages of firing rates and LFPs triggered on the onsets of saccades or onsets of fixations during free viewing of natural images (Fig. 2*A–D*). As reported in our previous study (Maldonado et al. 2008), the fixation-onset–triggered mean firing rate starts to rise at about 40 ms after fixation-onset and reaches its peak value at around 70 ms (Fig. 2*A*,*B*). The saccade-onset–triggered average also follows a similar time course. Although the peak height is slightly higher for the fixation-onset–triggered average, this difference is not significant (paired 2-tailed *t*-test; $P = 0.078$ for monkey D and $P = 0.053$ for monkey S). On the other hand, there is a clear difference between the LFP averages triggered on the fixation-onset and saccade-onset (Fig. 2*C*,*D*). For both trigger events, the LFP averages exhibit a sinusoidal waveform of about 1.5 cycles, but the saccade-onset–triggered LFP has a significantly larger amplitude than the fixation triggered LFP at the first positive deflection (paired 2-tailed *t*-test; $P < 0.0001$ for both animals). We note that the onset of a saccade and the onset of the following fixation are on average separated only by the saccade duration of 31 ms (monkey D) or 33 ms (monkey S). The LFP modulation, however, starts about 50 ms after saccade-onset, that is, during the early fixation period. The fact that the amplitude of the saccade-onset–triggered LFP is larger than the fixation-onset–triggered LFP (first peaks, respectively) indicates that the LFP modulations are more tightly coupled to the onsets of saccades than to the onsets of fixations.

The sinusoidal appearance of the LFP averages strongly indicates that the modulation of LFP activity after eye movements is on a specific time scale. To determine which time scale contributes most to the average LFP, we analyzed the phase consistency of the LFP activities across fixations (see Materials and Methods), resolved for frequencies in the range of 1–100 Hz. The phase consistency value for a given frequency is larger the more consistent the phase relationship of the signal in this frequency band is in relation to a given trigger event across trials. Therefore, the concentration of large phase consistency values in a specific frequency range indicates the presence of a time-locked response (either evoked or due to phase reset of ongoing oscillations) in a specific frequency range. As shown in Figure 2*E*,*F*, the largest phase consistency values are present in a narrow frequency range, which lies within the beta frequency band, centered at 16 Hz for monkey D and 13 Hz for monkey S.

The average firing rate and the average LFP show an interesting relationship: The first positive peak of the LFP response coincides with the onset of the change of the firing rate, while the following trough coincides with the peak of the firing rate (Fig. 3, top). To elucidate the details of this temporal relation between the various neuronal activities and the eye events, we examined how the latencies of the LFP and the spike responses depend on the duration of the saccades. For this purpose, we grouped S–F trials according to their saccade durations and calculated fixation-onset–triggered averages of LFP and firing rate separately for each of the groups (for details, see Material and Methods). For the visualization of the 2 variables, we plotted these averages as a function of time and

saccade duration (Fig. 3). Figure 3*A,B* shows that the onsets of the LFP modulations have a constant latency from saccade-onset (cyan oblique line), which clearly indicates that the LFP activity is locked to saccade-onset and not to fixation-onset. Interestingly, the onsets of the firing rate increase follow a similar pattern (Fig. 3*C,D*). However, as discussed below, we have indications that the origin of the locking to saccade-onset is different for the 2 signals.

For comparison, we also examined the changes of LFP and spiking activities around the onset of eye movements on a blank screen. The firing rates (Fig. 4*A,B*, saccade triggered: red and fixation triggered: blue) in the blank condition are in tendency lower than in the image condition (Fig. 4*A,B*, gray curves). In monkey D, the firing rates reach the rate level attained in the image condition at a later phase of the fixation period, being considerably lower in the early phase of the fixation period. The same holds true for monkey S, but here the firing rates are lower than in the image condition, with the largest difference at rate onset. By contrast, in the blank condition, the average LFPs triggered on saccade-onset (blue) and fixation-onset (red) (Fig. 4*C,D*) exhibit amplitude modulations that are at least as large as in the image condition (Fig. 4*C,D*, gray). Notably, in the blank condition, the time scales of the changes in the spike and LFP activities are slower than in the image condition. This can also be observed in the results of the phase consistency analysis of the LFPs (Fig. 4*E,F*): The maximum phase consistency values are concentrated at much lower frequencies (7.5 Hz for monkey D and 5.5 Hz for monkey S) in the blank condition (for consistent results in the dark, see also Rajkai et al. (2008)) as compared with the image condition (16 Hz for monkey D and 13 Hz for monkey S).

Since the experimental chamber was not completely dark in the blank condition, part of the observed responses may have been due to visual stimulation by the edges of the monitor screen. To examine this possibility, we calculated the average LFP and the mean firing rate separately for 2 classes of fixations: one comprising fixations around the center of the screen and the other fixations close to or at the edge of the screen. These classes were derived by sorting the S–F trials in descending order of the distances of their fixation positions to the nearest monitor edge. The top and the bottom quartiles of these S–F trials were selected as containing center fixations and edge fixations, respectively. As shown in Figure 5, the onset of the rate increase was either considerably delayed for the center fixations (Fig. 5*A*, monkey D, cyan) or the increase was almost completely suppressed (Fig. 5*B*, monkey S, cyan). This suggests that the initial part of the rate response may indeed be due to stimulation by the monitor edge. In fact, the relative change of the initial rate increase related to the edge fixations was as large as in the image condition (gray dashed curve). But we also observed a rate increase for the center fixations with some delay (in monkey D), suggesting that the eye movements as such can evoke (or induce) spiking activity without a visual stimulation. This is consistent with the report by Rajkai et al. (2008), where an increase in the multiunit activity was observed in response to eye movements performed in total darkness. On the other hand, we find that, in contrast to the firing rates, the amplitudes of the LFP modulations related to eye movements were neither diminished nor delayed for center fixations (Fig. 5*C,D*). Splitting the fixations into 2 classes reduced the sample size of the LFP responses and increased their variance. Neverthelss, the LFP averages for center fixation trials exhibit a similar timing and amplitude modulation as the LFPs for edge fixations. Taken together, these observations suggest that the early changes in the firing rates are related to visually evoked neuronal activity, while the changes in the LFPs (and likely also the later part of the rate responses) are coupled to the eye movements.

Phase Relation of Spikes to LFP

The result of the saccade duration–resolved analysis (Fig. 3) suggests that the latency of the visually evoked spiking activity is modulated by saccade-related neuronal activity, which

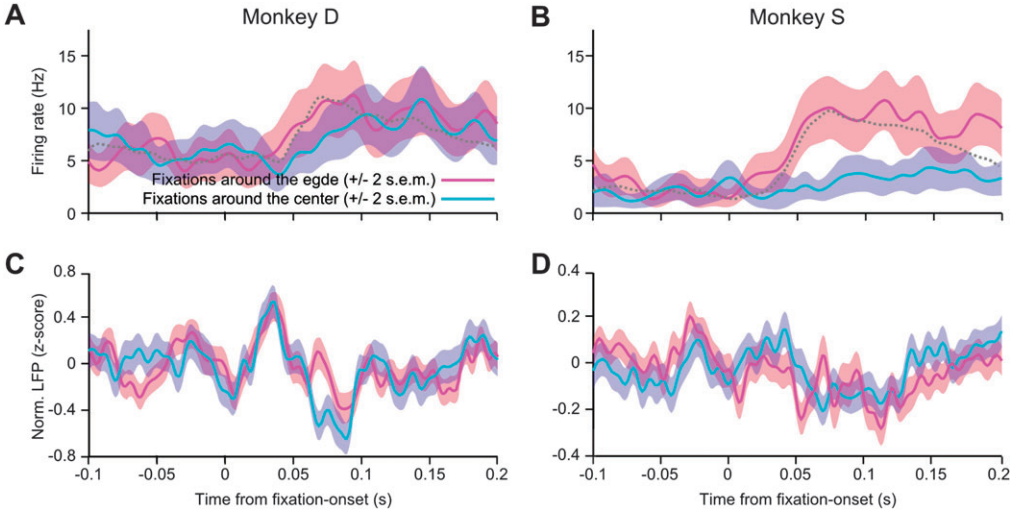

Figure 5. Firing rates and LFP activities related to eye-event onsets in the blank condition, calculated for the fixations around the center of the monitor screen and close to its edge. For the selection of center fixations and edge fixations, we sorted the S–F trials in the descending order of the distance between their fixation position and the nearest monitor edge. The fixations comprising the top and the bottom quartiles were selected as the center fixations and the edge fixations, respectively. (*A,B*) Mean firing rate triggered on fixation-onset, obtained from edge fixations (pink) or from center fixations (cyan). The color-shaded areas represent ±2 s.e.m. of the respective signals. For comparison, the mean firing rates from the image condition are also shown (gray dashed). However, for better comparison of the modulation of the responses in the different conditions, we shifted the firing rates from the image condition by a vertical offset such that their value at time 0 (i.e., fixation-onset) is equal to those of the edge fixations (pink). (*C,D*) LFP averages triggered on saccade-onset (time is shifted by median saccade duration as in Fig. 2). Color convention is same as for (*A,B*).

manifests itself in the LFP signals. To examine this possibility on a trial-by-trial basis, we studied the temporal relation of individual spikes in single trials to the changes in the background LFP activity. For a quantitative characterization of a potential temporal locking of the spikes to a specific phase of the LFP modulations, we examined the PLV (for details, see Materials and Methods and Fig. 6). The clear sinusoidal waveform of the average LFP justifies the usage of phase values as a reference for representation of specific timing relations between individual spikes and LFP modulations.

We first explored the locking of the spikes that occurred during the period where the firing rate and the LFP exhibited the largest changes, defined as the interval centered at the peak of PSTH and spanning one cycle of the dominant LFP frequency (see yellow area in Fig. 7*A*,*B*). To account for trivial locking that may be induced by the nonstationarity of the firing rate during this interval, we derived the significance of the PLV by use of a surrogate method (Random Shuffling Surrogate in Materials and Methods section). These surrogate data sets were generated by shuffling the spike trains across the S–F trials (while the LFPs remained unshuffled) to intentionally destroy the simultaneity of the spike trains and the LFP recordings. The PLV was evaluated from the surrogate set in the same way as done in the original data. From such repetitively generated surrogate data, we thus derived the PLV distribution reflecting independent data (Fig. 6). The empirical PLV (Fig. 7*C*,*G*, green bars) was then tested for its significance using this distribution (Fig. 7*C*,*G*, cyan bars marked ALL). We found locking of the spikes to the LFP well beyond the 0.1% significance level, also expressed in very high values of the SM (Fig. 7*E*,*I*, green bars). This is also directly visible in the comparison of the cycle histogram of the original spikes (Fig. 7*D*,*H* left, green bars) with the mean cycle histogram of the surrogate spike data (Fig. 7*D*,*H* left, cyan lines).

The results of the phase-locking analysis indicate that visually evoked spikes occur preferentially at a particular phase of the LFP modulations. Such phase locking may be the mechanism responsible for the occurrence of excess spike synchrony in particular for early response spikes. In fact, Maldonado et al. (2008) showed the occurrence of excess spike synchrony at around the onset of the visual response, that is, about 20 ms before the peak firing rate. Therefore, we

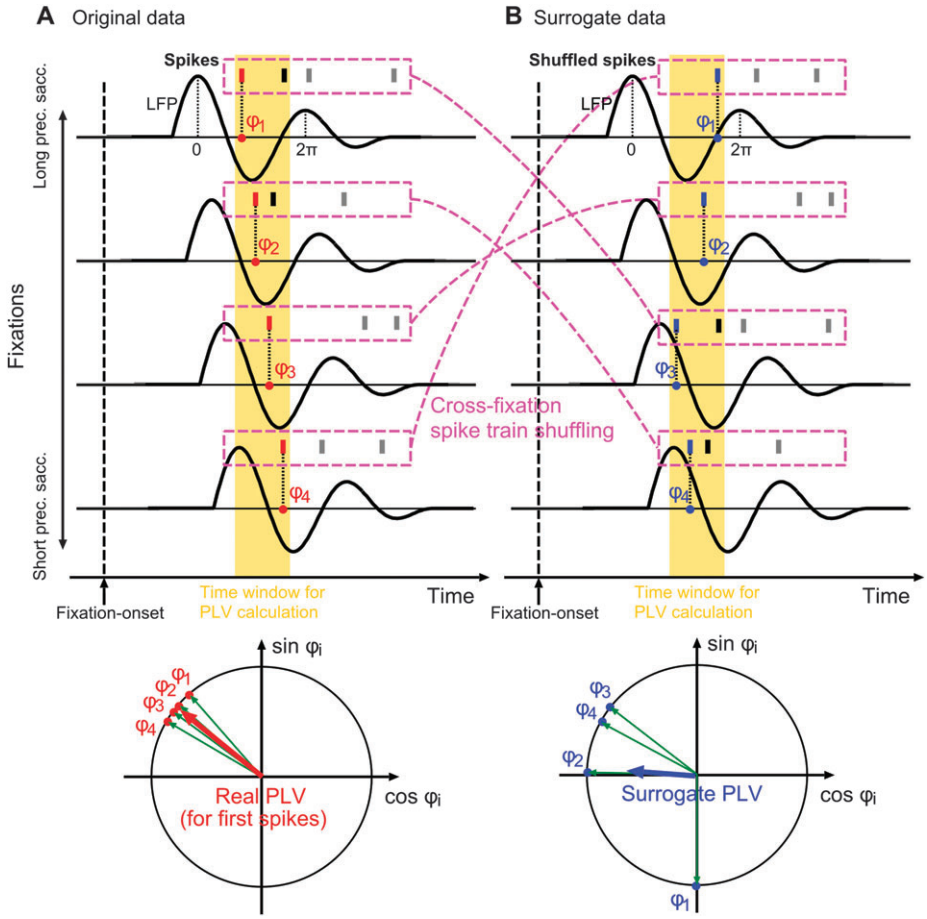

Figure 6. Schematic illustration of phase-locking analysis and generation of surrogate data. (*A*) Each row sketches data from one S–F trial around fixation-onset (dashed vertical line): LFP (black curve) and a simultaneously recorded spike train (vertical ticks). The phase-locking analysis is illustrated here for first spikes per trial (red ticks). To calculate the PLV, the LFP phases at spike times (red dots) are averaged by circular statistics (bottom panel). The length of the obtained average vector (red arrow) represents the empirical PLV. For illustration, the PLV is here computed within the prespecified time window (yellow area). For a time resolved phase–locking analysis, the window is slid in time and the PLV is calculated at each window position. To derive the locking tendency of all spikes within the window, the PLV may also be calculated on their basis (including the black spikes). (*B*) Illustration of the generation of the surrogate data for the significance test of the PLV. To estimate the PLV expected from independent LFP and spike signals, the spike trains are randomly shuffled across the S–F trials (pink arrows). The extracted phase values (blue dots) from these newly combined spikes and LFP signals serve to compute the surrogate PLV calculated in the same manner as for the original data.

repeated the phase-locking analysis with specific emphasis on spikes occurring at the onset of the rate response. Due to the relatively low firing rates of the neurons, the estimation of the onset of the rate change in single trials was not reliable. Therefore, we decided to simply focus on the first spike per trial after fixation-onset. The histogram of these spikes (Fig. 7*A,B*, red) indicates that they often occur shortly after fixation-onset. This is trivially explained by the first event delay distribution for a point process of a given (stationary) rate. These very early spikes are likely not to be caused by the visual input, given the propagation delay from the retina to V1 of about 35 ms in mammals (Livingstone et al. 1996; Schiller and Tehovnik 2001). Thus, we concentrated on the first spikes that are likely related to the visual input, by considering only the S–F trials that showed a first spike within the analysis window also used in the previous analysis (yellow marked areas in Fig. 7*A,B*). This time window captures the second peak of the first spike histogram, likely reflecting the early spikes of visual input. Note, we did not relabel the first spikes in relation to the beginning of this time interval but just discarded S–F trials in which the first spike did not occur in this time interval. Clearly, our selection of the first spikes is only a very rough estimate of the spikes potentially representing the onset of the responses and may be "contaminated" by spontaneous spikes that are not elicited by the stimulus. Therefore, we compared the PLV calculated for the set of the first spikes (1ST) to the PLV of the set of the second spikes (2ND). The latter were selected from the same time interval by corresponding criteria as for the 1ST spikes and independently from them. The result of this analysis shows a clear difference in the degree of phase locking between these 2 classes of spikes (Fig. 7*C,E,G,I*): Only 1ST spikes exhibit a significant phase locking with *P* values much smaller than 0.001, while the *P* values for 2ND spikes do not even reach a *P* value of 0.01.

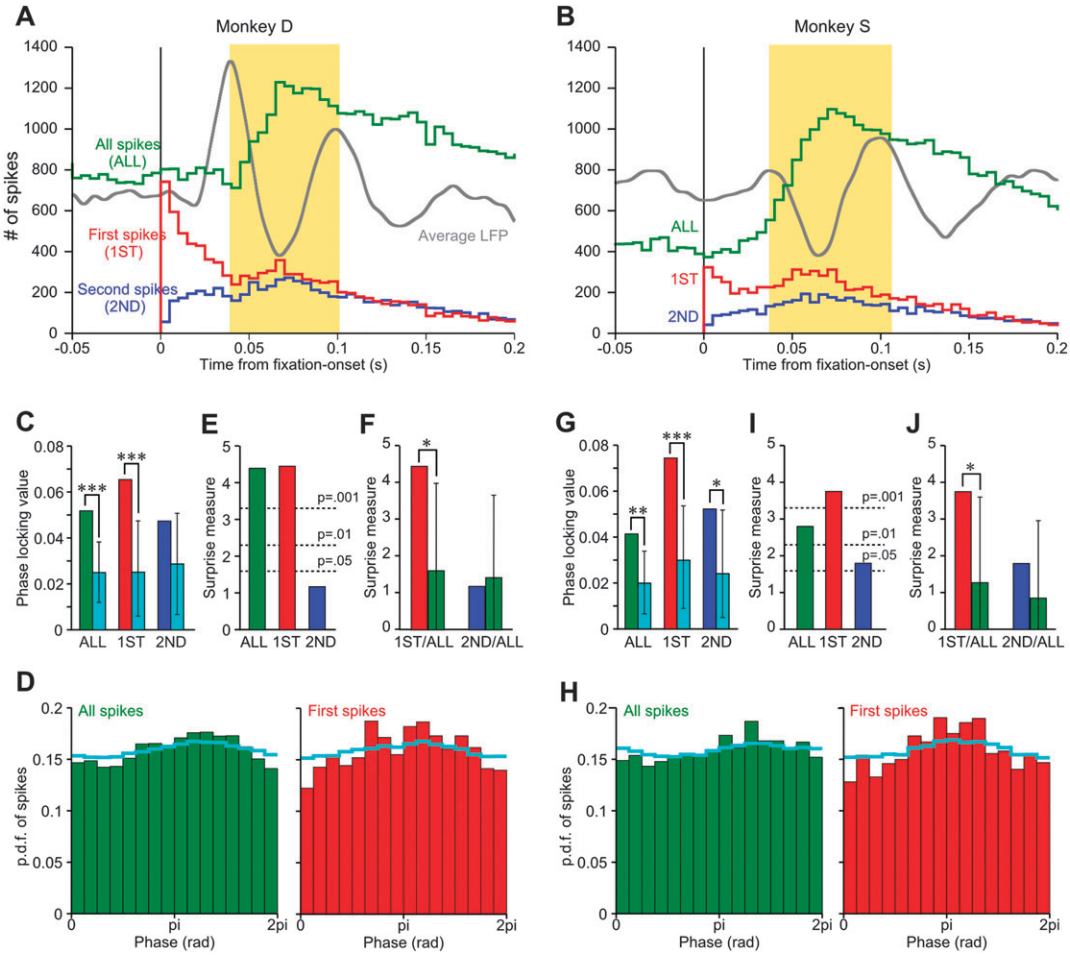

Figure 7. Phase locking of spikes of individual neurons to LFP modulations during fixation periods. Panels (*A,C,D,E,F*) and (*B,G,H,I,J*) show data of monkey D and S, respectively. (*A,B*) Spike histograms of different sets of spikes aligned to fixation-onset (bin width: 5 ms). The histogram of all spikes (ALL, green) is a binned and rescaled version of the mean firing rate in Figure 2. The histogram of the first spikes (1ST, red) represents the time-resolved counts of the first spikes occurring in each trial after fixation-onset. Correspondingly, the other histogram represents the counts of the second spikes (2ND, blue) in each trial after fixation-onset. The saccade-onset–triggered average LFP is also shown (gray curve, arbitrary units) to illustrate the temporal relationship between the spiking activities and the LFP. (*C,G*) PLV for respective sets of spikes (the same color convention as in (*A,B*)). PLVs are calculated within a time interval encompassing the largest changes in LFP and firing rate (yellow marked area in (*A,B*); for its definition, see Materials and Methods). To the right of each PLV is the mean of the surrogate PLVs (cyan) with the bar representing the 95 percentile of the surrogate PLV distribution. (*$p <$ 0.05, **$p < 0.01$, and ***$p < 0.001$.) (*D,H*) Period histograms of ALL spikes (left) and 1ST spikes (right) represented as a probability density function (p.d.f.). Cyan lines show the p.d.fs. of the corresponding surrogates. (*E,I*) Significance of the PLVs shown in (*C,G*) expressed in terms of the SM. Color convention is same as in (*A,B*) and (*C,G*). Dashed lines indicate the significance levels with different *P* values. (*F,J*) Comparison of the SMs for 1ST and 2ND spikes to the SMs for randomly resampled surrogate subsets of ALL spikes. The size (i.e., the number of spikes) of the surrogate subsets was matched to the size of 1ST or 2ND spikes. Green bars and the associated error bars represent the median and the 95 percentile of the SMs for the resampled ALL spikes, respectively.

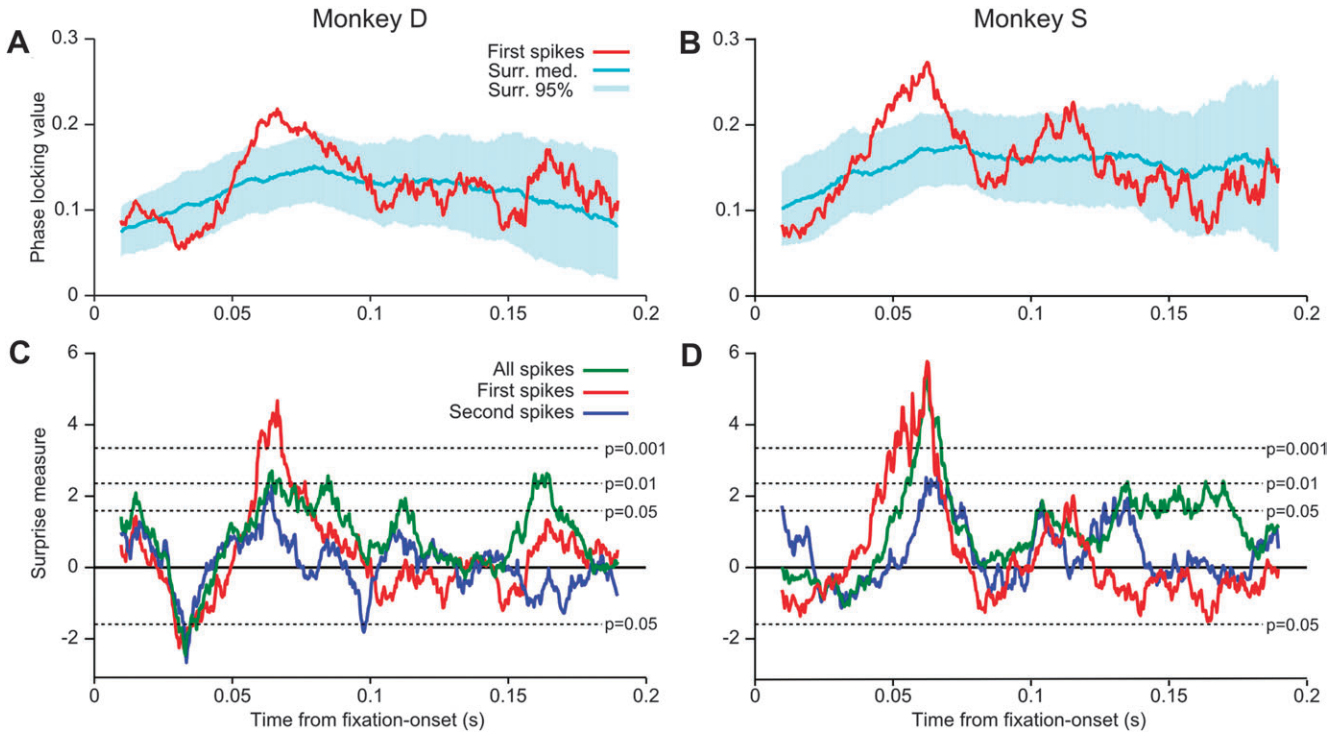

Figure 8. Time-resolved analysis of phase locking. Panels (*A*,*C*) and (*B*,*D*) show data of monkey D and monkey S, respectively. (*A*,*B*) PLV of the first spikes as a function of time relative to fixation-onset. PLVs calculated from the real data (red trace) are plotted with the PLVs form surrogate data, shown with the median value (cyan curve) and the 95 percentile of the PLV distribution (cyan area) at each time point. (*C*,*D*) Time-resolved SM of the PLV for the first (red), second (blue), and all (green spikes in the image condition). The dotted horizontal lines indicate different significance levels (2-tailed). All calculations were done in a sliding window manner with a time window of 20-ms width.

To further elucidate the potential special role of the first spikes after fixation-onset, we compared the significance of 1ST and 2ND spikes on the basis of resampling from ALL spikes. To this end we randomly selected the same number of spikes as the reference class from ALL spikes in the same time interval. For these randomly selected spikes, we also calculated the PLV and evaluated its significance in terms of SM by use of the above-mentioned trial shuffling surrogate method. This procedure was repeated 1000 times to yield the distribution of SMs. Figure 7*F*,*J* shows the comparison of the SMs of the 1ST (red) and 2ND (blue) spikes in comparison to the respective SMs from resampled ALL spikes (both in green). In both animals, the SM for 1ST spikes is significantly larger than the surrogate SMs, while the SM for 2ND spikes is within the 95 percentile of the surrogate SMs. Although both, 1ST and 2ND spikes, are subsets of ALL spikes, only the 1ST spikes are nevertheless significantly different from ALL spikes implying that these indeed comprise a special subset of spikes that exhibit phase locking to the LFP modulations in contrast to other spikes.

To examine whether the phase locking of spikes to the LFP modulations extends throughout the whole fixation period, we performed also a time resolved phase-locking analysis using a narrow sliding analysis window (20-ms width). This analysis was applied again separately for 1ST and 2ND spikes, as well as for ALL spikes. The time course of the PLVs of the 1ST spikes and the corresponding (random shuffling) surrogate are shown in Figure 8*A*,*B*. The PLV of 1ST spikes remains within the 95 percentile of the surrogate distribution for most of the fixation period but shows a highly significant increase ($P < 0.001$) at around 60 ms after fixation-onset (Fig. 8*C*,*D*). This indicates that the phase locking observed in Figure 7 is due to excess locking during a short, initial period. The timing of significant locking coincides with the negative peak of the LFP modulation and also with the second peak of the first spike histogram (Fig. 7*A*,*B*). The time course of the phase locking of 2ND spikes occurs with considerably lower significance values (Fig. 8*C*,*D*). This result confirms that the phase locking is highly selective for the first spikes in V1 at about 60 ms after the beginning of a fixation.

Mechanism of First Spike Phase Locking

The observed phase locking of early spikes is most likely due to the temporal modulation of neuronal excitability (Hopfield 1995; Mehta et al. 2002; Rajkai et al. 2008). The present analysis revealed an oscillatory LFP that was phase locked to saccade onset. LFPs result from synchronous trasmembrane currents in the population of neurons adjacent to the recording electrode, inward and outward currents causing negative and positive deflections, respectively. Most of the contributing currents result from EPSCs and IPSCs because these summate much more effectively than the rapidly alternating inward and outward currents of action potentials (Mitzdorf and Singer 1977, 1978, 1979, 1980, 1985). At a single unit level, this modulation is likely to be reflected in membrane potential modulations, since the LFP was shown to strongly correlate with the membrane potential (Lampl et al. 1999; Poulet and Petersen 2008; Okun et al. 2010). This leads to the interpretation that the time of occurrence of an output spike of a V1 neuron is determined by the interaction between its momentary excitability, which can be modeled as a fluctuating firing threshold of the neuron, and an additional visually driven, afferent input (Fig. 9*A*). The temporal jitter of the neuron's output spikes across trials is expected to be small—even when the excitatory drive is variable—if the 2 inputs intersect at the

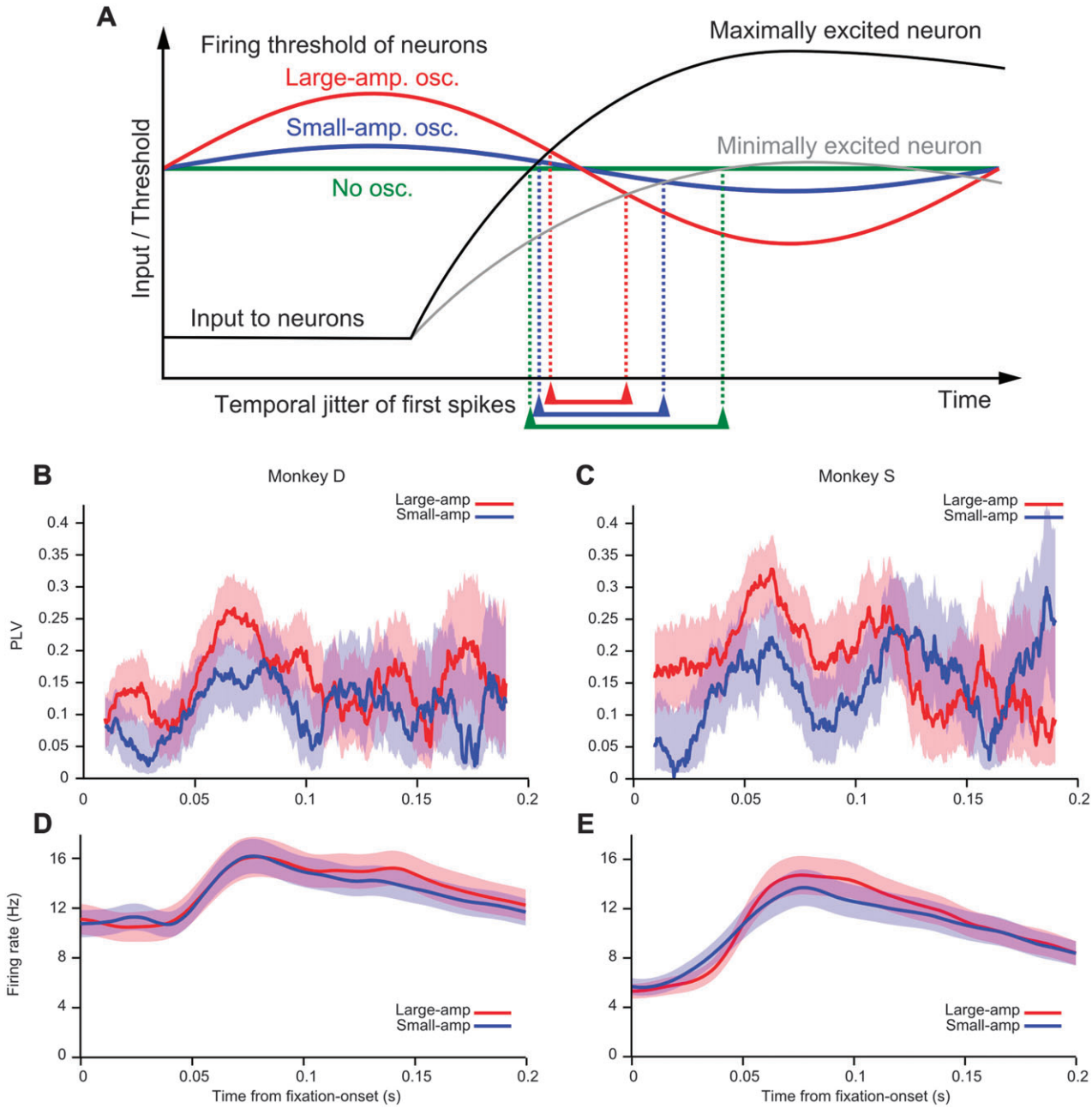

Figure 9. Influence of LFP amplitude on spike time precision. (*A*) Proposed model to account for spike timing precision based on the LFP modulation. Modulations of the field potentials are assumed to correlate with changes in the effective firing threshold of neurons (colored curves). Different levels of LFP amplitude modulation are shown in colors (red, blue, and green). 2 different temporal profiles of neuronal activation by sensory input are depicted as a black and gray curve. The crossing point of a neuronal activation curve with the effective firing threshold defines the time of the firing of the first spike (triangular marks on the time axis). The temporal jitter of the first spikes induced by different strength of neuronal activation depends on the amplitude of the threshold modulation. (*B–E*) Test of the model in experimental data (left column: monkey D, right column: monkey S). Fixation-triggered S–F trials were separated into 2 groups according to the amplitude of the first positive peak of the LFP response (50% largest [red] vs. 50% smallest [blue]) and were analyzed separately. The time resolved mean phase–locking value (*B*,*C*) and the time-dependent mean firing rate (*D*,*E*) are shown for the 2 groups. The shaded area in (*B*,*C*) represents 95% confidence interval of the PLV estimated by the trial shuffling method. The shaded areas in (*D*,*E*) represent ±2 s.e.m. of the respective signals.

steepest slope of the LFP. Thus, a first prediction of the model is that a larger degree of phase locking should be associated with larger LFP amplitudes as compared with cases with smaller LFP amplitudes.

To test this prediction, we separated S–F trials into 2 groups according to the size of the LFP response amplitude, with one group composed of trials of large LFP amplitudes and the other with small amplitudes (for details, see Materials and Methods). The comparison of the degree of phase locking of the first spikes of the 2 groups (Fig. 9*B*,*C*) reveals—as predicted—a higher degree of phase locking for the high amplitude group. On the contrary, the firing rates calculated separately for the 2 groups (Fig. 9*D*,*E*) do not show a difference in the strengths of the rate responses. Thus, a higher degree of phase locking is not associated with a higher firing rate. Consequently, the difference in the degree of phase locking can only be explained by a mere modulation of spike timing without an accompanying change in the firing rates of the neurons.

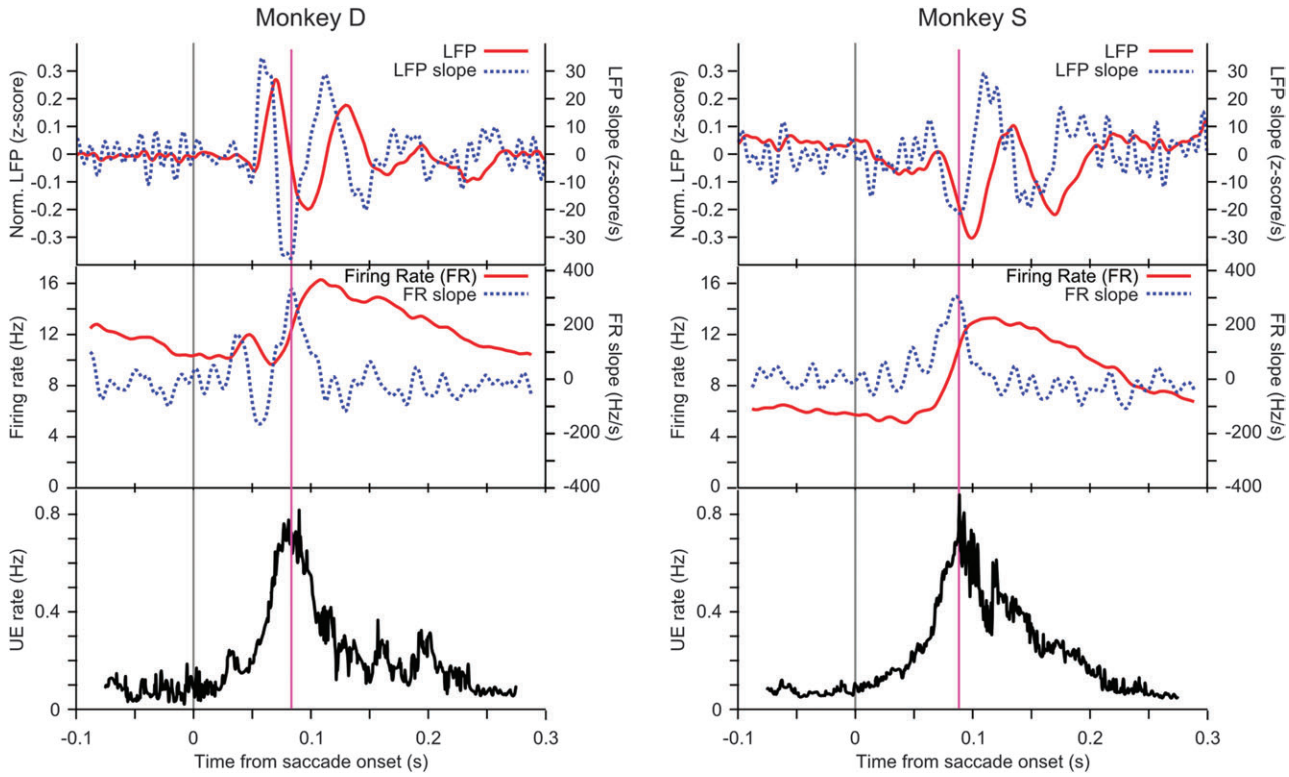

Figure 10. Temporal relationship between LFP, firing rate, and UE rate. Red solid and blue dashed curves in the top panel represent saccade-onset–triggered average LFP and its 1ST temporal derivative (dashed blue), respectively. The pink vertical line indicates the position of the negative peak of the derivative, which corresponds to the steepest negative slope of the LFP. It coincides with the peak of excess spike synchrony between neurons, measured as UE rate (bottom panel) as predicted by our model. The UE peak precedes the peak of the firing rates of the neurons but coincides with the timing of the fastest rate increase (middle panel).

A second prediction of the model is related to the timing of spike synchrony between neurons. Let us now consider a number of V1 neurons simultaneously, each receiving afferent inputs of different strengths due to, for example, differences in their tuning. Their time course of excitability, however, is expected to be very similar as suggested by the strong correlations between simultaneously recorded, nearby LFPs (Destexhe et al. 1999). As argued above, the temporal jitter of the output spikes of the neurons is expected to be smallest at the time of the steepest slope of the LFP, that is, at the point of inflexion. Thus, spikes of different neurons under the influence of similar excitability modulations should have a higher probability to coincide with each other around this point in time. To test this prediction, we calculated the time course of excess spike synchrony (UEs, as in Maldonado et al. 2008) across all possible pairs of simultaneously recorded neurons and compared it with the corresponding time course of the average LFP. As the model predicts, the peak of the excess spike synchrony coincides exactly with the steepest negative slope of the LFP, as illustrated by the coincidence of the peaks of the derivative of the LFP and of the UE rate (Fig. 10). Thus, our model is capable of explaining consistently the preferred locking of first spikes to the LFP phase as well as the occurrence and timing of excess spike synchrony. The peak of the excess spike synchrony precedes the peak of the firing rate (Maldonado et al. 2008) and coincides with the timing of the fastest rate increase (Fig. 10, middle row). This result suggests that the peak of the excess synchrony is due to enhanced synchronization between early visually evoked spikes, which is consistent with our model prediction emphasizing the contribution of first spikes to excess spike synchrony.

Discussion

Our results show that under a natural viewing condition, that is, when the animals perform self-initiated eye movements while viewing natural scene images, LFP modulations in the beta frequency range are initiated in V1 with the beginning of saccades, suggesting the arrival of an eye movement–related signal at this area. This signal appears to modulate the timing of the onset of visually evoked spiking activity during fixations, leading to a locking of these first spikes to a specific phase of the LFP modulation and thereby providing a mechanism for the synchronization of these spikes.

The phase locking of the first spikes is highly likely a reflection of the interaction between the visual input–related signal and the eye movement–related signal in V1. To elucidate this point, we examined data from the blank condition, where a blank frame was presented instead of natural scene images. We found that the initial increase in the firing rate after a saccadic eye movement is due to visual stimulation rather than due to eye movements (will be discussed in more detail below). On the other hand, the LFP modulations in the blank condition were as large as in the image condition, indicating that the LFP modulations after saccades are related to eye movements per se rather than to fixations. Based on these observations, we postulated a model for the mechanism of phase locking of spikes to the LFP as the interaction between afferent visual input and saccade-related modulation of excitability. This model correctly predicted the dependence of the strength of the phase locking on LFP amplitude as well as the timing of excess spike synchrony.

Origin of the LFP Modulation

The saccade-related LFP modulation is likely to reflect a corollary signal that is generated in association with eye movements. We find this LFP modulation to be present in both, the image and the blank condition (cmp. Bartlett et al. 1976). A corollary signal was suggested to result either as a feedback signal from extraocular muscles (Buisseret and Maffei 1977) or as an efferent copy (Purpura et al. 2003). The latter is likely to originate in the pontine reticular formation and to be related to the pontogeniculooccipital waves that accompany eye movements and are associated with excitability changes in the lateral geniculate nucleus and the visual cortex (Jeannerod et al. 1979). This corollary discharge has been proposed to serve as a mechanism to reset areas involved in visual processing by erasing the traces of the presaccadic image and by simultaneously raising excitability at the onset of the new fixation (Singer 1977; Rajkai et al. 2008; for a review, see Melloni et al. 2009). In addition, it had been postulated to reduce transmission of visually induced signals during saccades (saccadic suppression) to avoid interference with signals resulting from novel, postsaccadic input (Burr et al. 1994).

Whilst it can be asserted that LFP modulations reported here could be caused by the visually induced feed-forward input, 2 of our results argue against this possibility. First, the initial component of the LFP modulations occurs rather early (~20 ms after fixation-onset) to be caused by visually induced inputs. Second, during eye movements in the blank condition, the LFP modulations are still present with amplitudes and latencies comparable with those observed in the image condition (Fig. 4). Certainly, it cannot be ruled out that later components of the LFP modulations may contain contributions from visually induced inputs. In fact, the difference between the average LFP in the image and in the blank condition is larger for those later components. However, we contend that the earliest components are most relevant for the observed phase locking of first spikes because, according to our model, only the first excitatory change in neural excitability, which is reflected by the first negative slope of the LFP modulation, is crucial for generating the phase locking of the first spikes.

The biophysical origin of the LFP has been discussed to reflect coordinated synaptic input and slow intrinsic conductances (Mitzdorf 1985; Buzsaki 2006) in the local cortical network. Although this is a plausible assumption, there is yet no direct experimental validation of this view. Rather, it was shown that, while there is a strong correlation between the LFP and the simultaneously intracellularly measured membrane potential, the relation of the LFP to the output spiking activity of the cell is not as clear and in particular does not show a one-to-one relationship (Lampl et al. 1999; Poulet and Petersen 2008; Okun et al. 2010). This observation holds even more so for synchronous spike events—even if the membrane potentials of 2 cells correlate well, and in turn correlate with the LFP, the output spiking of these cells is not necessarily correlated (Poulet and Petersen 2008). This is consistent with our finding that the time course of the excess spike synchrony is not comodulating with the LFP modulation (Fig. 10). These results rather suggest that at occurrence times of excess spike synchrony additional input is available (in our case saccade-related excitability) as reflected by the LFP, thus leading to a nonlinear relation of LFP and output spike synchrony. This view is very much in agreement with the findings of Denker et al. (2010) and Denker et al. (2011), who showed that excess synchronous spike events (Grün et al. 2002a, 2002b) exhibit a stronger phase locking to the LFP than synchronous events occurring at chance level. The authors concluded that this excess spike synchrony and its preferred locking to the LFP is the result of an interaction of "background" oscillatory LFP and incoming packets of synchronous activity.

Another possible contribution to the observed LFP modulations is related to attention because of the tight coupling observed between the mechanisms controlling eye movements and attention (Corbetta et al. 1998; Everling 2007). It is well known that attentional mechanisms affect the responses of V1 cells and LFPs to simple visual stimuli (Motter 1993; Fries et al. 2001). However, it is quite difficult to dissociate attentional effects from eye movement–related effects. For this purpose, one would need to prepare a condition where animals make eye movements to either attended or nonattended stimuli, but even then the absence of attention cannot be fully substantiated just because the animals did make eye movements to the (putatively) nonattended stimuli. In the present study, we did not intend to introduce specific attentional changes but rather tried to keep the animals at a stationary attentional level (see Materials and Methods). Whilst we did not have a precise way to monitor their attentional state, we could measure brain activity related to voluntary, self-initiated eye movements, which were not driven by changes of the saliency in the visual input. It would be desirable to further manipulate top-down and bottom-up attentional states by exploiting certain appropriate tasks, but we believe that is reasonably regarded as beyond the scope of the present study and left to be explored in future studies.

Saccade-Related Signals in the Blank Condition

Examination of spiking activities in the blank condition enabled us to disentangle different components in the rate responses in relation to eye movements. We separated the fixations into center fixations (without visual stimulation) and edge fixations (likely associated with stimulation by the monitor edges) and found that for the edge fixations the modulation depth of the initial rate response and its timing corresponds to the type of response we found in the image condition, while the response appeared considerably delayed or was even diminished for the center fixations. In monkey D, a later increase in the firing rates occurred without visual stimulation. This is attributed to eye movements and in agreement with the findings by Rajkai et al. (2008). This late part of the response cannot be related to the phase locking that we observed in the image condition, since we demonstrated that this phase locking involves exclusively early visually induced spikes.

While a number of previous studies have reported eye movement–related changes in spiking activity in visual cortices (for a review, see Wurtz 2008), only a few have looked closely into the modulations of cortical field potentials during eye movements. One of these is a study by Rajkai et al. (2008) who studied the spiking activity (in form of MUA) and the CSD activity (derived from LFP recordings) in V1 in relation to voluntary eye movements in the dark. They found phase-locked CSD signals in the delta/theta frequency band (3–8 Hz) and a rate increase of the MUA in relation to fixation-onset, the latter occurring even in complete absence of visual stimulation. The conclusion of this study is that the modulation of the CSD reflects a modulation of the local neuronal ensemble in preparation of the visual inputs that would arrive in a stimulus

condition after fixation-onset. The rate changes they found are likely to be related to the eye movement as such. Our findings complement their results in 2 aspects. First, we confirmed found the phase-locked modulation of the LFP. The dominant frequency of this LFP modulation in the blank condition agrees well with that found by Rajkai et al. (2008). However, we observed a higher dominant frequency (beta range) during active exploration of natural scenes (i.e., the image condition). In addition, we were able to identify this response as locked to saccade-onset rather than to fixation-onset. This distinction could not be made in Rajkai et al. (2008) due to the low sampling rate of the eye movement recordings (70 Hz). Second, during self-initiated eye movements in the blank condition, we also find a late component of firing rate increase in a situation without any visual stimulation (center fixations). The timing of this component coincides with the first negative deflection of the phase-locked LFP modulation, supporting the hypothesis of a preparatory increase of excitability that interacts with the visually evoked activity. Rajkai et al. (2008) reported eye movement–related changes of the power of LFP oscillations in a wider frequency range, including beta and gamma frequency bands. This aspect, as well as the change in the dominant frequency of the phase-locked components as a function of experimental conditions, needs to be explored in future studies.

The Influence of Microsaccades

Recent studies support the view that microsaccades and saccades form a to saccade continuum because they share a common oculomotor generator (Martinez-Conde et al. 2009). In fact, Bosman et al. (2009) reported that microsaccades during prolonged fixations evoke or phase-reset LFP oscillations, similarly to our findings. Notably, they showed that the average LFP triggered on the onset of microsaccades exhibited modulations on the time scale of the delta/theta frequency band (Fig. 2*A* in Bosman et al. 2009) and also that the LFP shows phase locking to the onset of microsaccades in a wide frequency range spanning from the delta/theta band to the high gamma band (~80 Hz), with the most prominent locking around the beta band (Fig 3*A* in Bosman et al. 2009). The phase locking in higher frequencies than the beta band, which is missing in our observation, may be attributed in their study to the very strong neuronal activation (firing rates up to 100 Hz) caused by stimulation with high contrast gratings. Such a stimulation is known to evoke gamma band oscillations in the LFP and in the spiking activities (Juergens et al. 1999; Friedman-Hill et al. 2000; Berens et al. 2008), which might contribute to phase locking of the LFPs in the gamma band to the onset of microsaccades. The discrepancy in the dominant frequencies of the saccade-locked LFP modulations might be attributed to the difference of the experimental conditions, that is, free viewing of natural images in our study and fixating with attention to a peripheral target in Bosman et al. (2009). This point, however, needs to be clarified in future studies.

Given the above findings on microsaccade-related LFP changes, one need to consider to which extent microsaccades might have influenced our results. In fact, studies on humans have shown that microsaccades occur also during free viewing (Otero-Millan et al. 2008). However, the probability is small that we detected microsaccades since our threshold for saccade detection was set to 1°, which is a standard criterion for discrimination between microsaccades and regular saccades. On the other hand, Otero-Millan et al. (2008) also reported that microsaccades occur mainly at later stages during prolonged fixations and that the intervals between microsaccades and regular saccades are on the same order as those between 2 regular saccades. Given that our analysis was always performed in the initial 200 ms from fixation-onset and that the average intersaccade interval is about 300 ms, we can safely assume that LFP modulations occurring due to microsaccades had no or only a negligible effect on our results.

Implications for the concept of Active Vision

Recent studies have shown that the phase of ongoing oscillatory brain activity is relevant for behavioral performances. For example, Lakatos et al. (2008) reported that the reaction time in visual or auditory oddball tasks performed by monkeys is systematically modulated by the phase of delta band oscillations of CSD signals at the timing of stimulus onset. Mathewson et al. (2009) and Busch et al. (2009) reported that the performance of visual stimulus detection by human subjects is dependent on the timing of the stimulus presentation in relation to the phase of ongoing alpha band oscillations found in electroencephalography signals. Although the underlying physiological mechanism for these findings still needs to be revealed, it was suggested that the enhancement of sensory processing is due to synchronization of spikes through phase-locking to oscillatory signals (Fries et al. 2001; Womelsdorf et al. 2006). In our present study, we indeed found evidence that the synchronization of early response spikes during fixations (Maldonado et al. 2008) occurs at a particular phase of the background LFP modulation. We modeled a potential mechanism for such spike synchronization as an interaction between afferent visual inputs and efferent eye movement–related signals. The predictions by this model are consistent with our experimental observations. It may be speculated that this reflects a rather general mechanism that is not limited to periods of evoked LFP modulations but may also be operative during ongoing brain oscillations.

Another interesting possibility is that oscillations of different frequencies are concatenated and serve different functions. The slow component of the ongoing oscillations is likely to be related to a centrally generated rhythmic exploration process defining the sequence of saccades and microsaccades thereby providing an optimal discrete sampling of visual scenes (see Discussion and related references in Bosman et al. 2009). In fact, our preliminary results from a recent study suggest a coupling between the phase of delta band LFP oscillations, which is locked to the timing of eye movements and the amplitude of beta band LFP modulations, which in turn has an influence on spike timings (Ito et al. in preparation). Thus, such relationships between activities at different time scales suggest a hierarchical organization of brain signals in the temporal domain (Lisman and Idiart 1995; Lakatos et al. 2005; Canolty et al. 2006).

From considerations on the speed of visual information processing, it has been inferred that information about a visual stimulus should be extractable already from the very first spikes of a response and might be contained in the relative latency of these spikes (see Introduction; König et al. 1995; Gawne et al. 1996; Fries et al. 2001; VanRullen and Thorpe 2002; Kupper et al. 2005). Our findings provide support for the special role of first spikes and may therefore have implications for latency coding in primary visual cortex. Experimental studies that reported such latency coding typically have been conducted on either anesthetized (König et al. 1995; Fries et al. 2001.) or awake behaving but fixating animals (Gawne et al. 1996). In such conditions, the visual stimuli are presented at times not known to the subjects. Thus, the

neural system has no information about when visually induced activity reaches the cortex. In active vision, however, the visual system can make use of an internally generated signal, which is the saccade-related brief excitability modulation indexed by LFP changes. We showed that these modulations provide a framework to influence the timing of spikes by locking them to a specific phase of the modulations. Thus, active, natural vision with its frequent and self-initiated eye movements can make use of an effective mechanism for precise timing of spikes and synchronization of spikes between neurons, thus affecting downstream neurons efficiently (Abeles 1982; Alonso et al. 1996; Usrey and Reid 1999). Our study suggests a mechanism for the supportive role of eye movement–related signals in the active processing of visual inputs.

In summary, the present data suggest that saccade-related adjustments of spike timing may play an important role in visual processing in free-viewing conditions. How exactly information about stimulus features is encoded in these early, synchronized spikes requires further studies in which relations can be established between the RF locations of neurons, the visual stimuli and the early phases of the postsaccadic responses.

Funding

RIKEN Strategic Programs for R&D (to J.I.); Iniciativa Cientifica Milenio (P04-068F to P.M.); Volkswagen Stiftung (to P.M., W.S., and S.G.).

Notes

We thank Winrich Freiwald, Manabu Tanifuji, and Thomas Wachtler for inspiring discussions, and Denise Berger for her support in the initial phase of the project. *Conflict of Interest* : None declared.

References

Abeles M. 1982. Role of the cortical neuron: integrator or coincidence detector? Isr J Med Sci. 18:83–92.

Alonso JM, Usrey WM, Reid RC. 1996. Precisely correlated firing in cells of the lateral geniculate nucleus. Nature. 383:815–819.

Bartlett JR, Doty RW, Lee BB, Sr, Sakakura H. 1976. Influence of saccadic eye movements on geniculostriate excitability in normal monkeys. Exp Brain Res. 25:487–509.

Berens P, Keliris GA, Ecker AS, Logothetis NK, Tolias AS. 2008. Feature selectivity of the gamma-band of the local field potential in primate primary visual cortex. Front Neurosci. 2:199–207.

Bosman CA, Womelsdorf T, Desimone R, Fries P. 2009. A microsaccadic rhythm modulates gamma-band synchronization and behavior. J Neurosci. 29:9471–9480.

Buisseret P, Maffei L. 1977. Extraocular proprioceptive projections to the visual cortex. Exp Brain Res. 28:421–425.

Burr DC, Morrone MC, Ross J. 1994. Selective suppression of the magnocellular visual pathway during saccadic eye movements. Nature. 371:511–513.

Busch NA, Dubols J, VanRullen R. 2009. The phase of ongoing EEG oscillations predicts visual perception. J Neurosci. 29:7869–7876.

Buzsaki G. 2006. Rhythms of the brain. New York (NY): Oxford University Press.

Canolty R, Edwards E, Dalal S, Soltani M, Nagarajan S, Kirsch H, Berger MS, Barbaro NM, Knight RT. 2006. High gamma power is phase-locked to theta oscillations in human neocortex. Science. 393:1626–1628.

Corbetta M, Akbudak E, Conturo TE, Snyder AZ, Ollinger JM, Drury HA, Linenweber MR, Petersen SE, Raichle ME, Van Essen DC, et al. 1998. A common network of functional areas for attention and eye movements. Neuron. 21:761–773.

Csicsvari J, Jamieson B, Kensall EW, Buzsaki G. 2003. Mechanisms of gamma oscillations in the hippocampus of the behaving rat. Neuron. 37:311–322.

Denker M, Riehle A, Diesmann M, Grün S. 2010. Estimating the contribution of assembly activity to cortical dynamics from spike and population measures. J Comput Neurosci. 29:599–613.

Denker M, Roux S, Lindén H, Diesmann M, Riehle A, Grün S. 2011. The local field potential reflects surplus spike synchrony. Cereb Cortex. (in press).

Destexhe A, Contreras D, Steriade M. 1999. Spatiotemporal analysis of local field potentials and unit discharges in cat cerebral cortex during natural wake and sleep states. J Neurosci. 19:4595–4608.

Everling S. 2007. Where do I look? From attention to action in the frontal eye field. Neuron. 56:417–419.

Friedman-Hill S, Maldonado PE, Gray CM. 2000. Dynamics of striate cortical activity in the alert macaque: I. Incidence and stimulus-dependence of gamma-band neuronal oscillations. Cereb Cortex. 10:1105–1116.

Fries P, Neuenschwander S, Engel AK, Goebel R, Singer W. 2001. Rapid feature selective neuronal synchronization through correlated latency shifting. Nat Neurosci. 4:194–200.

Gallant JL, Connor CE, Van Essen DC. 1998. Neural activity in areas V1, V2 and V4 during free viewing of natural scenes compared to controlled viewing. Neuroreport. 9:2153–2158.

Gattass R, Sausa AP, Rosa MG. 1987. Visual topography of V1 in the Cebus monkey. J Comp Neurol. 22:529–548.

Gawne TJ, Kjaer TW, Richmond BJ. 1996. Latency: another potential code for feature binding in striate cortex. J Neurophysiol. 76:1356–1360.

Gray CM, Maldonado PE, Wilson M, McNaughton B. 1995. Tetrodes markedly improve the reliability and yield of multiple single-unit isolation from multi-unit recordings in cat striate cortex. J Neurosci Methods. 63:43–54.

Grün S, Diesmann M, Aertsen A. 2002a. Unitary events in multiple single-neuron spiking activity: I. Detection and significance. Neural Comput. 14:43–80.

Grün S, Diesmann M, Aertsen A. 2002b. Unitary events in multiple single-neuron spiking activity: II. Nonstationary data. Neural Comput. 14:81–119.

Grün S. 2009. Data-driven significance estimation of precise spike correlation. J Neurophysiol. 101:1126–1140.

Hopfield JJ. 1995. Pattern recognition computation using action potential timing for stimulus representation. Nature. 376:33–36.

Huxter JR, Senior TJ, Allen K, Csicsvari J. 2008. Theta phase-specific codes for two-dimensional position, trajectory and heading in the hippocampus. Nature Neurosci. 11:587–594.

Jacobs J, Kahana MJ, Ekstrom AD, Fried I. 2007. Brain oscillations control timing of single-neuron activity in humans. J Neurosci. 27:3839–3844.

Jeannerod M, Kennedy H, Magnin M. 1979. Corollary discharge: its possible implications in visual and oculomotor interactions. Neuropsychologia. 17:241–258.

Judge SJ, Richmond BJ, Chu FC. 1980. Implantation of magnetic search coils for measurement of eye position: an improved method. Vision Res. 20:535–538.

Juergens E, Guettler A, Eckhorn R. 1999. Visual stimulation elicits locked and induced gamma oscillations in monkey intracortical- and EEG-potentials, but not in human EEG. Exp Brain Res. 129:247–259.

Kayser C, Montemurro MA, Logothetis NK, Panzeri S. 2009. Spike-phase coding boosts and stabilizes information carried by spatial and temporal spike patterns. Neuron. 61:597–608.

Kirchner H, Thorpe SJ. 2006. Ultra-rapid object detection with saccadic eye movements: visual processing speed revisited. Vision Res. 46:1762–1776.

König R, Engel AK, Orelfsema PR, Singer W. 1995. How precise is neuronal synchronization? Neural Comput. 7:469–485.

Kupper R, Gewaltig M-O, Korner U, Korner E. 2005. Spike-latency codes and the effect of saccades. Neurocomputing. 65–66:189–194.

Lakatos P, Karmos G, Mehta AD, Ulbert I, Schroeder CE. 2008. Entrainment of neuronal oscillations as a mechanism of attentional selection. Science. 320:110–113.

Lakatos P, Shah A, Knuth K, Ulbert I, Karmos G, Schroeder CE. 2005. An oscillatory hierarchy controlling neuronal excitability and stimulus processing in the auditory cortex. J Neurophysiol. 94:1904–1911.

Lampl I, Reichova I, Ferster D. 1999. Synchronous membrane potential fluctuations in neurons of the cat visual cortex. Neuron. 22:361–374.
Le Van Quyen M, Foucher J, Lachaux J-P, Rodriguez E, Lutz A, Martinerie J, Varela FJ. 2001. Comparison of Hilbert transform and wavelet methods for the analysis of neuronal synchrony. J Neurosci Methods. 111:83–98.
Lee H, Simpson GV, Logothetis NK, Rainer G. 2005. Phase locking of single neuron activity to theta oscillations during working memory in monkey extrastriate visual cortex. Neuron. 45:147–156.
Lisman J, Idiart M. 1995. Storage of 7 ± 2 short term memories in oscillatory subcycles. Science. 267:1512–1515.
Livingstone MS, Freeman DC, Hubel DH. 1996. Visual responses in V1 of freely viewing monkeys. Cold Spring Harb Symp Quant Biol. 61:27–37.
MacEvoy SP, Hanks TD, Paradiso MA. 2008. Macaque V1 activity during natural vision: effects of natural scenes and saccades. J Neurophysiol. 99:460–472.
Maldonado P, Babul C, Singer W, Rodriguez E, Berger D, Grün S. 2008. Synchronization of neuronal responses in primary visual cortex of monkeys viewing natural images. J Neurophysiol. 100: 1523–1532.
Martinez-Conde S, Macknik SL, Troncoso XG, Hubel DH. 2009. Microsaccades: a neurophysiological analysis. Trends Neurosci. 32:463–475.
Mathewson KE, Gratton G, Fabiani M, Beck DM, Ro T. 2009. To see or not to see: prestimulus α phase predicts visual awareness. J Neurosci. 29:2725–2732.
Mehta MR, Lee AK, Wilson MA. 2002. Role of experience and oscillations in transforming a rate code into a temporal code. Nature. 417:741–746.
Melloni L, Schwiedrzik CM, Rodriguez E, Singer W. 2009. (Micro)-Saccades, corollary activity and cortical oscillations. Trends Cogn Sci. 13:239–245.
Mitzdorf U. 1985. Current source-density method and application in cat cerebral cortex: investigation of evoked potentials and EEG phenomena. Physiol Rev. 65:37–100.
Mitzdorf U, Singer W. 1977. Laminar segregation of afferents to lateral geniculate nucleus of the cat: An analysis of current source density. J Neurophysiol. 40:203–1244.
Mitzdorf U, Singer W. 1978. Prominent excitatory pathways in the cat visual cortex (A 17 and A 18): a current source density analysis of electrically evoked potentials. Exp Brain Res. 33:371–394.
Mitzdorf U, Singer W. 1979. Excitatory synaptic ensemble properties in the visual cortex of the macaque monkey: a current source density analysis of electrically evoked potentials. J Comp Neurol. 187:71–84.
Mitzdorf U, Singer W. 1980. Monocular activation of visual cortex in normal and monacularly deprived cates: an analysis of evoked potentials. J Physiol (Lond.). 304:203–220.
Montemurro M, Rasch MJ, Murayama Y, Logothetis NK, Panzeri S. 2008. Phase-of-firing coding of natural visual stimuli in primary visual cortex. Curr Biol. 18:375–380.
Motter BC. 1993. Focal attention produces spatially selective processing in visual cortical areas V1, V2, and V4 in the presence of competing stimuli. J Neurophysiol. 70:909–919.
O'Keefe J, Recce ML. 1993. Phase relationship between hippocampal place units and the EEG theta rhythm. Hippocampus. 3:317–330.
Okun M, Maim A, Lampl I. 2010. The subthreshold relation between cortical local field potential and neuronal firing unveiled by intracellular recordings in awake rats. J Neurosci. 30:4440–4448.
Olshausen BA, Field DJ. 2005. How close are we to understanding V1? Neural Comput. 17:1665–1699.
Otero-Millan J, Troncoso XG, Macknik SL, Serrano-Pedraza I, Martinez-Conde S. 2008. Saccades and microsaccades during visual fixation, exploration, and search: foundations for a common saccadic generator. J Vision. 8(21):1–18.
Palm C, Aertsen A, Gerstein GL. 1988. On the significance of correlations among neuronal spike trains. Biol Cybern. 59:1–11.
Poulet JF, Petersen CC. 2008. Internal brain state regulates membrane potential synchrony in barrel cortex of behaving mice. Nature. 454:881–885.
Purpura KP, Kalik SF, Schiff ND. 2003. Analysis of perisaccadic field potentials in the occipitotemporal pathway during active vision. J Neurophysiol. 90:3455–3478.
Rajkai C, Lakatos R, Chen CM, Pincze Z, Karmos G, Schroeder CE. 2008. Transient cortical excitation at the onset of visual fixations. Cereb Cortex. 18:200–209.
Schiller PH, Tehovnik EJ. 2001. Look and see: how the brain moves your eyes about. Prog Brain Res. 134:127–142.
Singer W. 1977. Control of thalamic transmission by corticofugal and ascending reticular pathways in the visual system. Physiol Rev. 57:386–420.
Usrey WM, Reid RC. 1999. Synchronous activity in the visual system. Annu Rev Physiol. 61:435–456.
VanRullen R, Thorpe SJ. 2002. Surfing a spike wave down the ventral stream. Vision Res. 42:2593–2615.
Vinje WE, Gallant JL. 2000. Sparse coding and decorrelation in primary visual cortex during natural vision. Science. 287:1273–1276.
Volgushev M, Chistiakova M, Singer W. 1998. Modification of discharge patterns of neocortical neurons by induced oscillations of the membrane potential. Neuroscience. 83:15–25.
Womelsdorf T, Fries P, Mitra PP, Desimone R. 2006. Gamma-band synchronization in visual cortex predicts speed of change detection. Nature. 439:733–736.
Wurtz R. 2008. Neuronal mechanisms of visual stability. Vision Res. 48:2070–2089.